JOURNAL OF APPLIED ELECTROCHEMISTRY 22 (1992) 1121–1128

Electrochemical impedance spectroscopy of small Ni–Cd sealed batteries: application to state of charge determinations

Ph. BLANCHARD

SAFT, Alkaline Batteries Research Laboratory, 111, Bd A. Daney, 33074 – Bordeaux Cedex, France

Received 25 September 1991; revised 26 March 1992

Electrochemical impedance spectroscopy measurements have been carried out using small 0.85 A h cylindrical sealed cells at various states of charge. Evolution of impedance as a function of the charge or discharge current has been studied in the 0–0.85 A range and a method which allows an approximate state of charge to be determined has been developed.

1. Introduction

The search for an electrochemical impedance spectroscopy (EIS) based method which would allow the determination of the state of charge of Ni–Cd batteries has been the aim of much work [1–5]. However most of these studies involved the use of zero current impedance measurements. Under these operating conditions, impedance does not vary greatly as a function of the state of charge, except close to the end of discharge. For this reason, state of charge could not be easily determined.

The aim of this work was to seek another technique allowing more accurate measurement. A current (0.85 A) which roughly corresponds to the most common operating conditions encountered using this type of cell was therefore chosen. Measurements were carried out either during charge or discharge. In order to get a better understanding of the impedance origins, some measurements were also carried out using other current values.

2. Experimental method

The 0.85 A h VSE AA batteries tested contained a foam positive electrode and a plastic bonded negative electrode. Before EIS measurements were carried out, the batteries were subjected to a limited number of cycles (less than 5). Impedance was measured both during a 0.85 A charge (at different times corresponding to various states of charge i.e. 0%, 50%, 100% and 150%) and during discharge at the same rate (approximately at 90%, 75%, 50% and 25% states of charge). At the end of the charge batteries were allowed to rest at open circuit for 1 to 5 h before discharge spectra were recorded. In order to facilitate understanding of the spectra, additional measurements were also carried out, both at open circuit and also during charge and discharge at other current densities.

Measurements were carried out using a Solartron Schlumberger system including a 1286 potentiostat and a 1250 transfer function analyser. Current regulation was used in which a 25 mA alternating current, in a 1 kHz–25 mHz frequency range was superimposed on the direct current used for the charge or the discharge (generally 0.85 A). The internal calibration resistor value was set to 100 mΩ which was the lowest value available on the system. A 10 Hz low pass filter was switched on as soon as the frequency became lower than this value. From 3 to 100 cycles were achieved at each frequency, depending on its value, before the impedance was calculated. An oscilloscope was also used to check current and voltage signals. In order to minimize the perturbations arising from external connnections, a special holder was used which allowed separation of the current circuit from the voltage measurement circuit.

Under these operating conditions, each spectrum determination lasted approximately 4 to 5 mins. This duration corresponds, for the charge and discharge rates used in this study, to a charge variation close to 7 to 10%. Owing to the strong dependence of the impedance on the state of charge, when the remaining capacity in the battery falls down to less than 15%, all the measurements carried out in these conditions were discarded in order to limit drift-generated distortion of the diagrams. Data were collected on a plotter or recorded on a microcomputer for further mathematical treatments.

3. Data analysis

Impedance data were analysed using a fitting program which allowed each spectrum to be decomposed into elementary loops [6]. Spectra are basically composed of different capacitive half circles which differ from conventional *RC* loops by the fact that their centres are not located on the real axis of the Nyquist complex plane plot. This phenomenon was fitted using the Cole and Cole method [7] based upon a symmetrical dispersion of a capacitance value as a function of the frequency according to the following equation:

$$C_{(\omega)} = \frac{(RC)^{1-\alpha}\omega^{-\alpha}}{R} \times \left[\cos\left(\frac{\alpha\pi}{2}\right) - j\sin\left(\frac{\alpha\pi}{2}\right)\right] \quad (1)$$

0021-891X

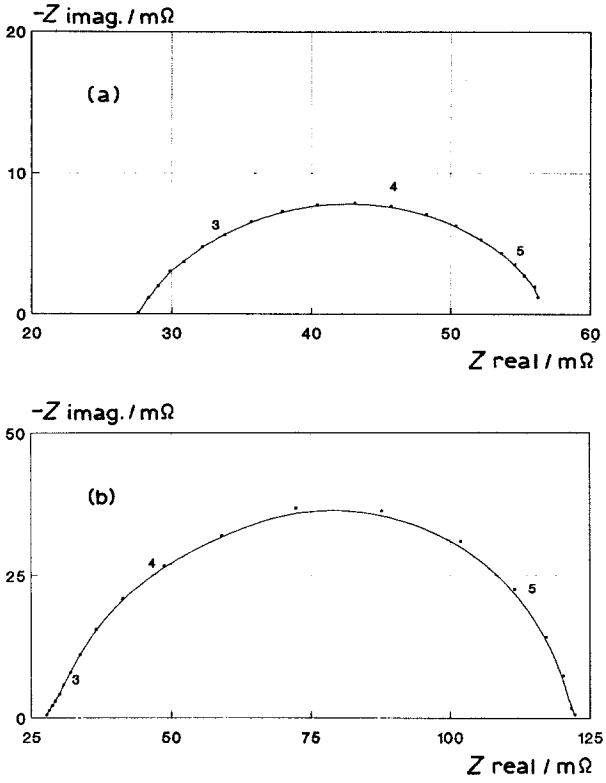

Fig. 1. Impedance of VSEAA cells during charge at 0.85 A. (a) 10% state of charge, (b) 63% state of charge.

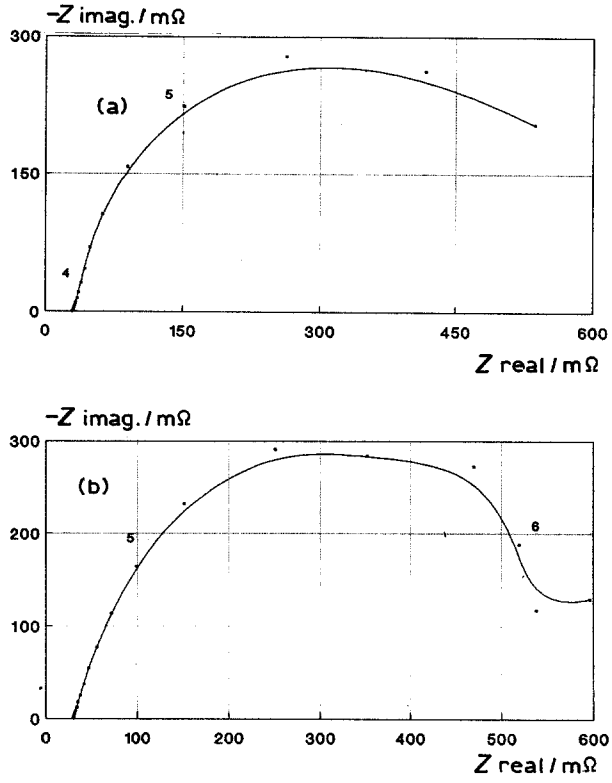

Fig. 2. Impedance of VSEAA cells during charge at 0.85 A. (a) 114% state of charge, (b) 157% state of charge.

where $C_{(\omega)}$ stands for the capacitance value at a $\omega/2\pi$ frequency, R is the resistance associated with the loop and α is the phase angle between the diameter of the half-circle and the real axis.

Although it is still difficult to associate this mathematical representation to a particular physical phenomenon, by using simulated diagrams it is possible to deduce that the method takes correctly into account both the shape of the diagrams and the distribution of frequencies on the diagrams.

In this study the fitting program was mainly applied to the determination of parameters R_t (charge transfer resistance) and C_{dl} (double layer capacitance) which are associated with the second loop observed during charge and discharge. The frequency range used to fit each diagram was chosen so that the standard deviation was minimal.

4. Results

4.1 *Impedance during charges*

During the charge of a battery, impedance diagrams are mainly composed of two capacitive loops (Figs 1 and 2). The correspondence between labels and frequency on the impedance plots is given in Table 1.

- A high frequency loop ($F > 100$ Hz) which does not appear to depend on the state of charge. As its contribution to the overall impedance is quite low and as it is not very well separated from the second loop, it was neglected in this study. The resistance value, R_∞, which arises from the electrolyte and different internal connections was measured at the high frequency intercept of the complex plane plot with the real axis, approximately 1 kHz. It was generally included in a 25–30 mΩ range (Table 2) and was found to remain fairly constant during charge. However, during overcharge a slight increase was noticed, which was attributed to oxygen evolution on the positive electrode forming bubbles in the electrolyte.
- A low frequency loop observed in the 100–0.1 Hz frequency range. Results of R_t, C_{dl} and α fittings collected in Table 2 clearly show an increase in R_t as the state of charge increases from 0 to 100%, and then a decrease in this parameter during overcharge. Among the reasons for this R_t drop during overcharge, the temperature rise and the change from the main electrochemical reaction to a secondary reaction (e.g. oxygen evolution reaction on the positive electrode, oxygen reduction on the negative electrode) are likely. To fully explain this R_t drop will require further work.

The double layer capacitance value C_{dl} increases from

Table 1. Correspondence between labels and frequency on impedance plots

Label	*Frequency/Hz*
1	10000
2	1000
3	100
4	10
5	1
6	0.1

Table 2. Impedance data of different VEAA cells during charge and discharge at 0.85 A

Cell number	*State of charge/%*	*Voltage/V*	R_∞/mΩ	R_t/mΩ	C_{dl}/F	*Angle /deg.*	$Z_{(1\,Hz)}$ /mΩ	$Z_{(0.4\,Hz)}$ /mΩ
Impedance during discharge								
9	91	1.27	23.7	9	3.8	−12	32.89	33.22
	74	1.23	24	8.6	3.7	−11	33.56	33.95
	48	1.22	25.2	10.5	2.5	−21	36.51	37.30
	22	1.186	28.9	20	1.2	−36	47.68	49.60
	5	1.1	30.4	–	–	–	80.84	95.71
16	89	1.233	32.4	7.51	4	−4	41.22	41.94
	44	1.203	34.9	10	2.3	−21	46.64	47.63
	16	1.151	39.4	35	0.72	−49	67.86	71.55
	4	1.09	41.1	60	0.66	−52	92.76	103.55
17	91	1.244	23.9	7.54	4.2	−4	32.57	32.45
	73	1.2	25.12	8.6	3.3	−14	34.44	34.54
	45	1.194	27.7	9.9	2.65	−15	39.97	40.71
	18	1.158	30.9	23.8	1.09	−42	52.59	55.34
Impedance during charge								
21	8	1.39	33.8	29.9	0.327	−34	61.08	62.00
	49	1.44	32.9	65.8	0.733	−19	92.56	97.30
	99	1.585	34.7	453	0.621	−31	251.94	419.62
	148	1.575	34.5	1343	0.843	−2.4	217.94	490.05
20	10	1.4	27.6	30	0.3	−35	54.71	56.06
	63	1.46	27.7	95	0.46	−15	113.85	120.33
	114	1.62	29.1	560	0.55	0	269.89	492.17
	157	1.54	29.4	730	1	−7	191.75	384.18
41	9	1.39	27.8	34.3	0.297	−38	54.50	56.39
	53	1.44	27.5	62.5	0.51	−21	82.88	86.38
	106	1.61	29.3	680	0.58	−4	265.04	512.72
	158	1.48	29.1	460	1.49	−1	138.60	268.41

approximately 0.3 to 1.5 F during charge and overcharge. At the present time no satisfactory explanation can be given for this phenomenon.

In order to gain more information about the electrochemical origins of the diagrams and, particularly, to verify if the second loop is related to a charge transfer phenomenon, some diagrams were also recorded, at an approximately 50% state of charge, using different charge rates: C rate (0.85 A), $C/2$ rate (0.425 A), $C/5$ rate and $C/10$ rate. Compared to the C rate spectrum, these diagrams differ mainly in the diameter of the second capacitive loop i.e. in R_t values (Figs 3 and 4). Results from the interpolations, collected in Table 3, clearly show that the result of the multiplication of the R_t value by the current I at each rate varies from 20 to 40 mV when the charge rate increases from $C/10$ to C. R_tI values measured at low current densities (e.g. $C/10$ rate) may thus be attributed to a reversible or mixed electrochemical process which is gradually transformed into an irreversible (or Tafelian) process, characterized by constant R_tI values, when the current increases.

Open circuit potentials were also measured at about 50% state of charge. A comparison between these values and those measured during charge at different rates (Table 3) allowed the origins of the observed overvoltages to be investigated. Thus, the ohmic drop ($R_\infty I$) which arises from electrolyte and connections seems to account, in the total overvoltage, to a lesser extent than the faradaic polarization. It must be noted that, as R_t is not constant through the range of current densities, a single impedance measurement does not allow the faradaic overvoltage to be directly obtained (Appendix 1); this can only be estimated by subtraction of the ohmic drop from the total overvoltage. The

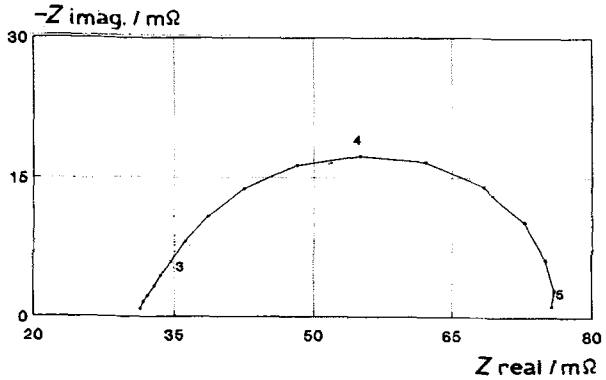

Fig. 3. Impedance spectrum during a C rate charge (state of charge close to 50%).

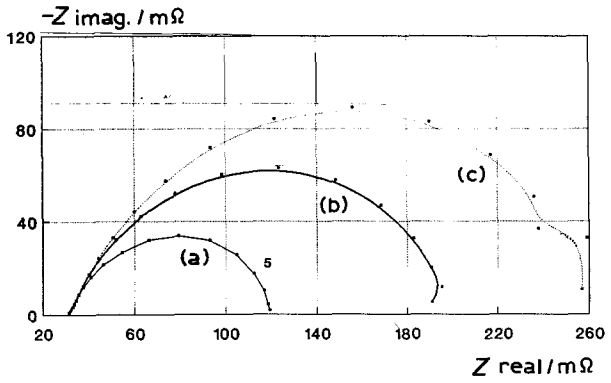

Fig. 4. Impedance spectra during charges at different rates (state of charge close to 50%). (a) $C/2$, (b) $C/5$ and (c) $C/10$.

reason why the polarization of the cell, from which the contribution of the ohmic drop has been removed, does not vary as much as expected from the R_tI value (e.g. 92 mV/decade) has not been explained.

4.2 *Impedance during discharge*

From a general point of view, during discharge, EIS diagrams appear to contain 3 capacitive time constants (Figs 5 and 6):

- a high frequency loop ($F > 100$ Hz) which appears to be similar to that observed in the same frequency range during charge. This loop was not fitted;
- a second loop observed in the 100–0.1 Hz frequency range, depending on the degree of discharge;
- at low frequencies ($F < 0.1$ Hz), a third loop is observed when the available capacity remaining in the battery becomes lower than 50%. This loop was not fitted because of the unfavourable conditions where it is encountered (low frequency range, low state of charge).

Moreover, it must be noted that the EIS diagrams recorded during discharge are flattened on the real axis of the complex plane plots. This may be due to the low impedance values compared to those observed during charge (in these conditions the first and second loop become less distinctive) and to the existence of 3 time constants instead of 2.

4.2.1. Evolution of electrolyte resistance during discharge. During discharge, the resistance corresponding to electrolyte and internal connections increases by approximately 8 to 10 mΩ (Table 2). This is probably due to a decrease of the electrolyte concentration in a given part of the battery (probably in the negative electrode or the separator) or to a loss of electrode conductivity. It must also be noted that the R_∞ value is lower at the beginning of the discharge than it is at the end of the charge; this phenomenon may be due to oxygen consumption during the open circuit period which decreases the bubble content of the electrolyte, or to relaxation processes, e.g. diffusion, which allow the electrolyte concentration to reequilibrate within the different parts of the cell.

4.2.2. Evolution of the second capacitive loop. Table 2 gives R_t, C_{dl} and α values for different times during the discharge (from 90% available capacity down to 15%). They show that R_t increases only slightly at the beginning of the discharge and then more drastically when the capacity which remains in the battery becomes lower than 25%. The C_{dl} value decreases from 4 to 1 F during the discharge.

As for the study of the charge process, voltage and impedance measurements were also carried out at various rates (between C and $C/10$) using half-discharged batteries (Figs 7 and 8). Table 3, where all the results have been collected, shows that R_tI varies from 4 to 8 mV depending on the discharge rate. At low current densities these values may also be attributed to a reversible or mixed activation process. On the other hand, at high current densities, the fact that no Tafelian zone can be observed probably indicates that the discharge reaction is controlled by a diffusion process or by the conductivity of active material. At the C rate, the R_t drop accounts for nearly 25% of the total cell polarization. This percentage becomes higher when the discharge rate increases.

4.3. *Application of EIS to the state of charge determination*

In order to compare the results of the zero current technique with those obtained in this study, some measurements were also carried out at open circuit,

Table 3. Impedance data during charge and discharge at different rates (states of charge close to 50%)

Current intensity	*State of charge*/%	*Cell voltage*/V	*Open circuit voltage*/V	R_∞ /mΩ	R_t /mΩ	C_{dl}/F	*Ohmic drop*/mV	R_tI /mV	*Faradaic pol.*/mV
Charge									
C (0.850 A)	42	1.465	1.294	31.3	47.2	0.336	26.6	40.1	144.4
$C/2$ (0.425 A)	52	1.441	1.297	31.3	92.8	0.414	13.3	39.4	130.7
$C/5$ (0.170 A)	54	1.42	1.298	31.3	183.7	0.887	5.3	31.2	116.7
$C/10$(0.850 A)	58	1.407	1.3	31.4	225.9	0.648	2.7	19	104.3
Discharge									
C (−0.850 A)	58	1.202	1.3	28.8	9.3	2.82	24.6	7.9	73.4
$C/2$ (−0.425 A)	51	1.247	1.297	29.5	14.7	2.94	12.5	6.2	37.5
$C/5$ (−0.170 A)	47	1.261	1.296	29.7	28.4	3.49	5	4.8	30
$C/10$(−0.850 A)	44	1.271	1.294	29.4	47.3	4.29	2.5	4	20.5

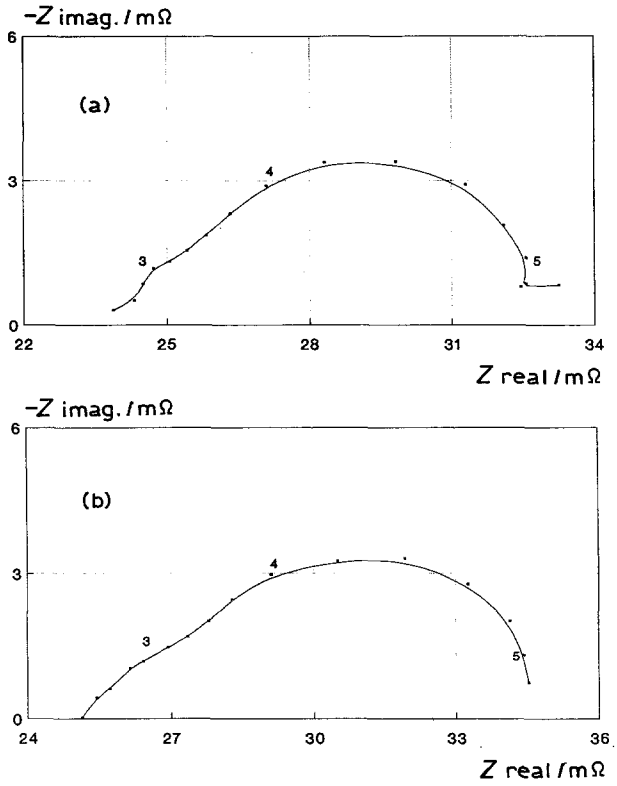

Fig. 5. Impedance of VSEAA cells during discharge at 0.85 A. (a) 91% available capacity, (b) 73% available capacity.

both at the charged state and at the end of the discharge (1 V cut-off voltage). Diagrams obtained (Figure 9) display quite different shapes but the impedance modulus measured in the 1–0.1 Hz range (this frequency range was chosen both because it corresponds to the second capacitive loop and because measure-

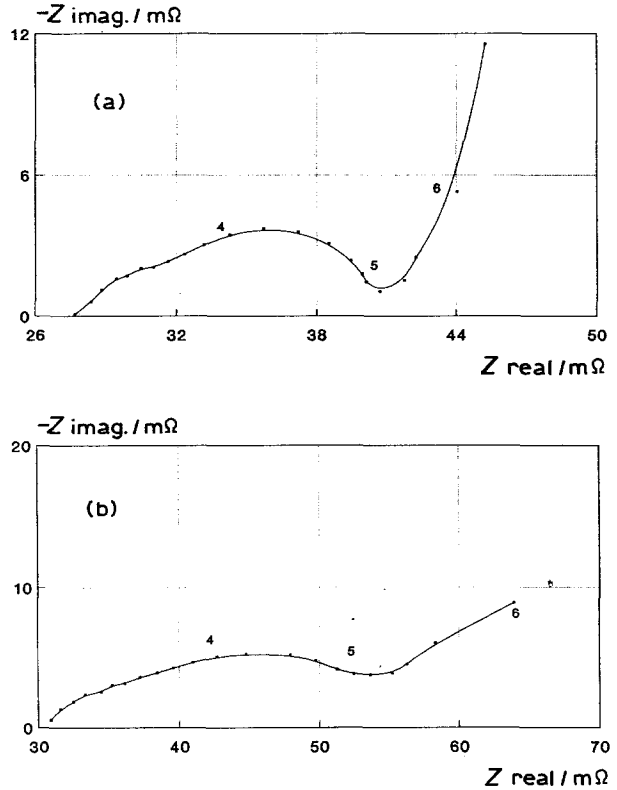

Fig. 6. Impedance of VSEAA cells during discharge at 0.85 A. (a) 45% available capacity, (b) 18% available capacity.

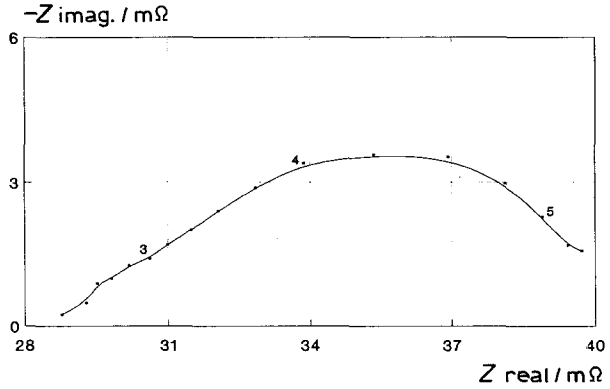

Fig. 7. Impedance spectrum during a C rate discharge (available capacity close to 50%).

ments in this range can easily and quickly be carried out using a single frequency analysis system) are approximately the same in both cases (Table 4). Moreover, because of the flattened shape of the diagram related to the discharged state, fittings are difficult to carry out and R_t cannot be determined with good accuracy and reliability. This confirms that EIS at zero current is not a suitable technique to measure the state of charge of a Ni–Cd battery.

Concerning measurements at a 0.85 A charge or discharge current, the values of the impedances at 1 Hz ($Z_{1\,Hz}$) and 0.4 Hz ($Z_{0.4\,Hz}$) have been calculated in Table 2; these two parameters as well as R_t and C_{dl} obtained from the interpolations have also been plotted as a function of the state of charge on Figs 10 and 11, respectively, for the charge and the discharge processes.

From these curves, it is seen that:

- during the charge, all R_t, $Z_{1\,Hz}$ and $Z_{0.4\,Hz}$ values increase when the charged capacity increases up to 100%, and then decrease during overcharge;
- C_{dl} increases regularly during charge and overcharge; and
- during the discharge, all these parameters increase.

This agrees well with the modifications of the polarization curves of both electrodes as a function of the state of charge, if one assumes that the measured impedance accounts for the vectorial sum of the impedances, i.e. the slope of the polarization curve of each

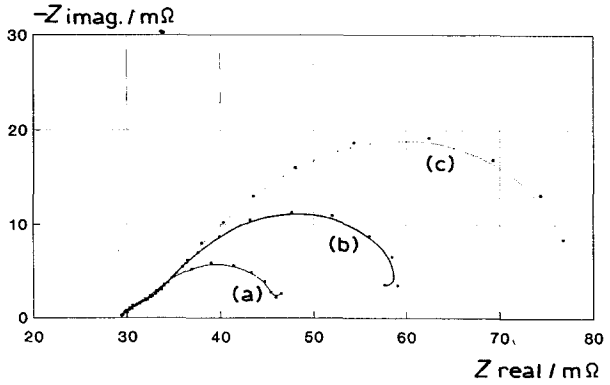

Fig. 8. Impedance spectra during discharges at different rates (available capacity close to 50%). (a) $C/2$, (b) $C/5$ and (c) $C/10$.

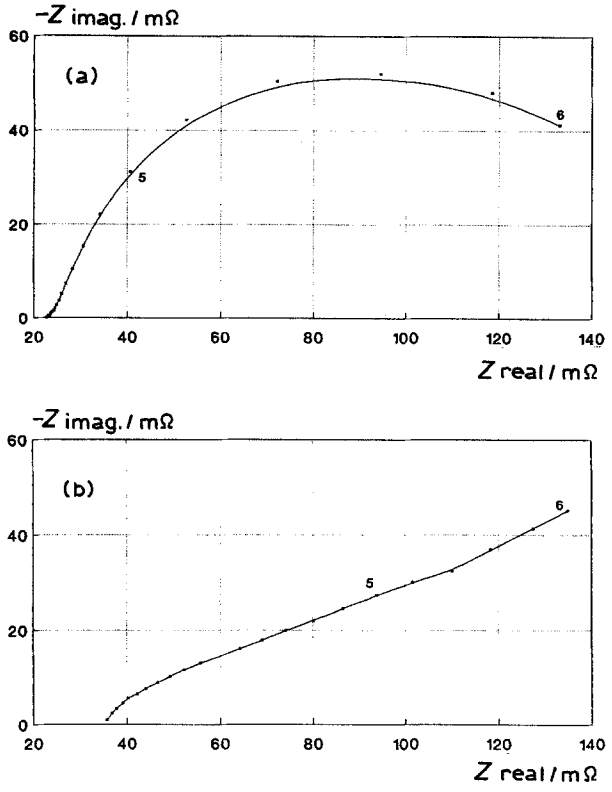

Fig. 9. Impedance spectra at zero current; (a) after a 1 h and 10 min charge at 0.85 A, (b) after a C rate discharge using a 1 V cut-off voltage.

electrode. Indeed, as the reaction goes on, less and less active material is available to react, leading to an increase in the current density on the unreacted electrode material.

The 1 Hz measurements, which do not need any fitting operation and can be rapidly carried out (e.g. every 10 to 15 s), appear to be representative of the capacity which is available in the battery. It only needs the current intensity to be kept at 0.85 A during the measurement period. In these conditions (but other operating conditions e.g. current or frequency could also be chosen for more convenience),if the impedance becomes greater than 200 mΩ during the charge, the battery may be considered fully charged. The state of charge determination may also be achieved by detecting the moment when the impedance starts to decrease. In other operating conditions (e.g. in the case of battery packs, where thermal effects can be quite different from those encountered using single cells) this must, however, be verified. On the other hand, during discharge, an increase in the 1 Hz impedance above a critical value of 60 mΩ indicates that approximately only 15% of the initial capacity is still available. For less discharged states (i.e. for depths of discharge between 0 and 80%) impedance is not strongly dependent on the state of charge, even if the R_∞ contribution is subtracted from $Z_{1\,Hz}$ or $Z_{0.4\,Hz}$. In this case, it is highly preferable to correlate the state of charge to C_{dl}, since a linear relationship can be observed between these two parameters.

However, to ensure complete reliability, these methods still need to be checked under other operating conditions. Particularly, the effects of temperature, ageing of the battery, as well as consequences of fragmented discharges or varying rest periods should be studied. Also, when changing from one electrode manufacturing technology to another, recalibration of the technique would have to be carried out.

5. Conclusions

In this study, the impedance of small cylindrical sealed cells was analysed during charge and discharge using different currents and states of charge. EIS diagrams obtained in these conditions display two or three time constants but mathematical interpolations were only carried out on the second capacitive loop, leading to accurate determination of R_t and C_{dl}. Evolution of $R_t I$ as a function of the current showed that the second capacitive loop may reasonably be attributed to a charge transfer reaction.

Concerning the state of charge determination, it may be assumed that:

- the electrolyte resistance does not vary sufficiently; and
- R_t and C_{dl} vary both as a function of the state of charge and of the applied current.

Under the given operating conditions, techniques which allow the determination an approximate state of charge can be proposed.

For example, if the current intensity is kept at 0.85 A, which corresponds to C rate for the type of batteries tested in this study, by measuring the impedance modulus at 1 Hz it is possible to detect either the moment when the battery is fully charged if measurements have been carried out during charge, or the moment when only 15% to 20% of the initial capacity is still available if measurements have been carried out during discharge.

During discharge, the available capacity of the battery may be estimated in a more accurate and reliable way by calculating the C_{dl} value. However this requires EIS measurements to be carried out over a

Table 4. Impedance data for charged and discharged cells at zero current

Cell number	*State of charge/%*	*Voltage/V*	R_∞ /mΩ	R_t /mΩ	C_{dl} /F	*Angle* /deg.	$Z_{(1\,Hz)}$ /mΩ	$Z_{(0.4\,Hz)}$ /mΩ
17	100	1.352	22.7	132	4.5	−12	51.1	88
9	100	1.381	23.7	760	5	−2	55.8	124.8
20	0	1.21	30				80.38	93.4
21	0	1.194	35.7				89.9	105.8

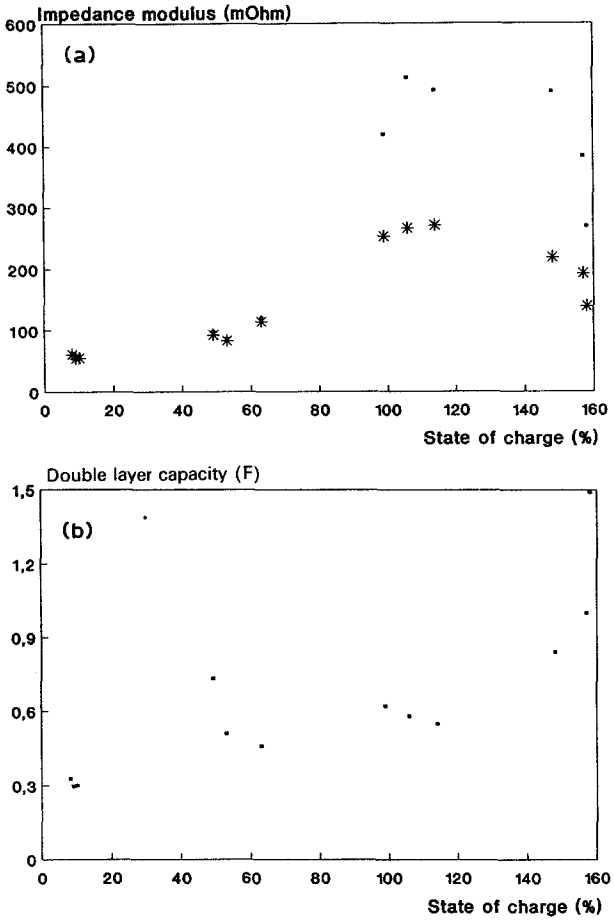

Fig. 10. Evolution of different impedance parameters during C rate charge. a: (*) Z at 1 Hz, (■) Z at 0.4 Hz; b: (■) C_{dl}.

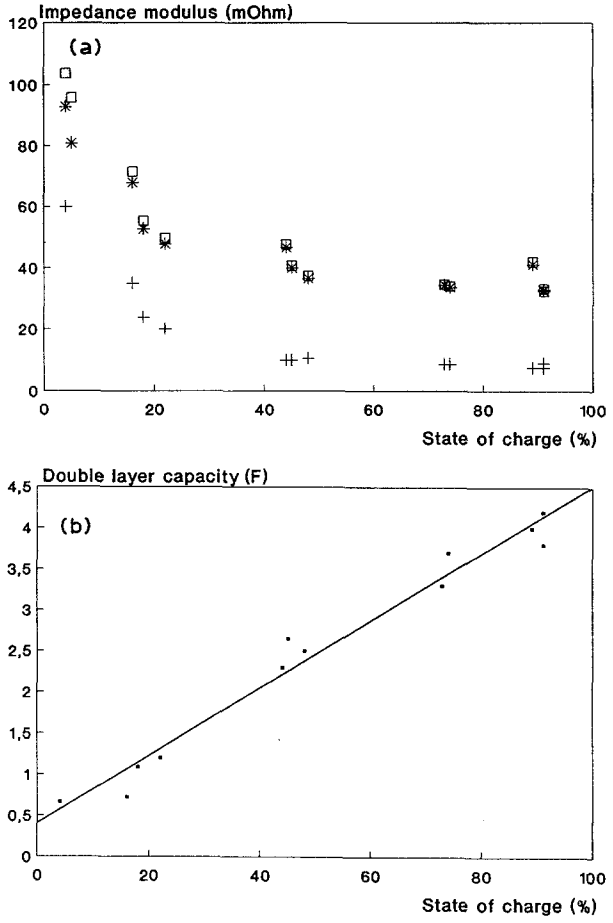

Fig. 11. Evolution of different impedance parameters during C rate discharge. a: (+) R_t, (*) Z at 1 Hz, (□) Z at 0.4 Hz; b: (■) C_{dl}.

wide range of frequencies in order to allow the fitting of this parameter.

Compared to other methods based on EIS determination at zero current, the techniques described in this paper appear to be more sensitive and accurate. However at this stage of the study, additional work is still necessary in order to make the method reliable and check its influence on the performances of the battery (capacity, cycle life . . .). This may also lead to a better understanding of the cell electrochemical processes.

References

[1] S. Sathyanarayana, S. Venugopalan and M. L. Gopikanth, *J. Appl. Electrochem.* **9** (1979), 125–39.
[2] M. Hughes, R. T. Barton, S. A. G. R. Karunathilaka, N. A. Hampson and R. Leek, *ibid.* **15** (1985), 129–37.
[3] M. A. Reid, Proceedings of the 174th meeting of the Electrochemical Society, Fall meeting, abstr. 81 (1988) p. 122.
[4] K. A. Murugesamoorthi, Y. J. Kim, S. Srinivasan and A. J. Appleby, *ibid.* p. 124.
[5] W. G. Marshall, R. Leek, N. A. Hampson and G. R. Lovelock, *J. Power Sources* **13** (1984), 75–81.
[6] Ph. Blanchard, J. Courtot-Coupez, contract IFREMER/UBO 84/7578, Brest (1985).
[7] K. S. Cole and R. H. Cole, *J. Chem. Phys.* **19** (1941), 341.

Appendix 1

From a general point of view, the current I which flows through an electrode polarized at a given potential E, can be expressed using the following equation:

$$I = I_0 \left\{ \frac{C_{red}}{C^*_{red}} \exp\left[\frac{\alpha nF}{RT}(E - E_{eq})\right] - \frac{C_{ox}}{C^*_{ox}} \exp\left[\frac{-(1-\alpha)nF}{RT}(E - E_{eq})\right]\right\} \quad (1)$$

where I_0 is the exchange current, E_{eq} the equilibrium potential, α the charge transfer coefficient, C_{red} and C_{ox} are, respectively, the reduced and the oxidized species at the electrode–solution interface and C^*_{red} and C^*_{ox} the reduced and oxidized species in the solution bulk.

If mass transport is neglected, which in the case of our study seems to be a realistic assumption as no diffusion loop was observed on the EIS diagrams, Equation 1 simplifies to Equation 2:

$$I = I_0 \left\{ \exp\left[\frac{\alpha nF}{RT}(E - E_{eq})\right] - \exp\left[\frac{-(1-\alpha)nF}{RT}(E - E_{eq})\right]\right\} \quad (2)$$

This leads to an I/E curve which displays different shapes depending on current density or overvoltage values.

- At low current densities (or low overvoltage values), the reaction undergoes a reversible process and the curve can generally be considered as a straight line with a R_∞ and R_t depending slope. In this case, the

electrode potential at a given current, I, is directly related to E_{eq} through Equation 3:

$$E_I = E_{eq} + (R_\infty + R_t)I \quad (3)$$

- At higher values of current density or overvoltage, the electrochemcial process is irreversible (or Tafelian) and the curve has an exponential shape. It can be shown that in this range R_t. I has a constant value. The relationship between E and I is then:

$$E_I = E_{eq} + I\left[R_\infty + 2.3R_t \log\left(\frac{I}{I_0}\right)\right] \quad (4)$$

Thus, obtaining a value for the faradaic overvoltage from a single impedance measurement basically implies that I_o value is known.

In the case of a battery, one must also consider that:

- Cathodic and anodic reactions do not belong to the same electrochemical system and, when the circuit is opened an exchange current does not really exist. The self-discharge current observed probably corresponds to the exchange current (or corrosion current) of one of the electrodes, the limiting electrode, and can be caused by different simultaneous reactions (e.g. NO_2^-/NO_3^- related reactions, oxygen evolution on Ni(III) oxides). In this way, self discharge current differs from I_o mainly by the fact that it cannot be considered as a constant parameter.
- On both electrodes, more than one electrochemical reaction can take place simultaneously. For example, during overcharge, and to a lesser extent during charge, oxygen evolution takes place at the positive electrode.

Acknowledgements

The author gratefully acknowledges M. Keddam and LP 15 CNRS, Paris, France, for helpful discussions.